Notch ligand activity is modulated by glycosphingolipid membrane composition in *Drosophila melanogaster*

Sophie Hamel,[1] Jacques Fantini,[2] and François Schweisguth[1]

[1]Institut Pasteur, Centre National de la Recherche Scientifique URA2578, 75724 Paris, Cedex 15, France
[2]Centre National de la Recherche Scientifique UMR 6231, Faculté St. Jérome, University of Aix-Marseille II and III, 13397 Marseille, Cedex 20, France

Endocytosis of the transmembrane ligands Delta (Dl) and Serrate (Ser) is required for the proper activation of Notch receptors. The E3 ubiquitin ligases Mindbomb1 (Mib1) and Neuralized (Neur) regulate the ubiquitination of Dl and Ser and thereby promote both ligand endocytosis and Notch receptor activation. In this study, we identify the *α1,4-N-acetylgalactosaminyltransferase-1* (*α4GT1*) gene as a gain of function suppressor of Mib1 inhibition. Expression of *α4GT1* suppressed the signaling and endocytosis defects of Dl and Ser resulting from the inhibition of *mib1* and/or *neur* activity. Genetic and biochemical evidence indicate that *α4GT1* plays a regulatory but nonessential function in Notch signaling via the synthesis of a specific glycosphingolipid (GSL), N5, produced by α4GT1. Furthermore, we show that the extracellular domain of Ser interacts with GSLs in vitro via a conserved GSL-binding motif, raising the possibility that direct GSL–protein interactions modulate the endocytosis of Notch ligands. Together, our data indicate that specific GSLs modulate the signaling activity of Notch ligands.

Introduction

The plasma membrane includes structurally diverse lipids and proteins that are spatially distributed in a heterogenous manner to form dynamic nanoscale assemblies (Hancock, 2006; Lingwood and Simons, 2010) that appear to be poised to cluster (Lingwood et al., 2008). Dynamic changes in the spatial organization of these domains may critically alter cell–cell signaling (Lajoie et al., 2009).

Cell–cell signaling mediated by Notch receptors regulates a wide range of developmental processes, and perturbations of Notch signaling activity underlie various human diseases. The molecular mechanism of Notch signaling is remarkably simple. Notch is a transmembrane protein with an intracellular domain corresponding to a transcriptional coactivator and with an extracellular ligand-binding domain. After interaction of Notch with its extracellular ligands, intramembrane proteolytic cleavage of Notch results in the release of the intracellular domain from the membrane and transcriptional activation of Notch target genes. Activation of Notch is thus irreversible, and a plethora of post-translational regulatory mechanisms control this irreversible step (for reviews see Bray, 2006; Fortini, 2009; Kopan and Ilagan, 2009; Tien et al., 2009). One key mechanism involves ubiquitination of the Notch ligands. In *Drosophila melanogaster*, Notch is activated in trans by the transmembrane proteins Delta (Dl) and Serrate (Ser). Genetic studies have indicated that ubiquitination of Dl and Ser by E3 ubiquitin ligases of the Mindbomb (Mib1) and/or Neuralized (Neur) is essential for Notch receptor activation in signal-receiving cells (for review see Le Borgne et al., 2005a). Mib1 is a conserved RING finger E3 ubiquitin ligase required for the internalization and/or endosomal sorting of Notch ligands (Itoh et al., 2003; Lai et al., 2005; Le Borgne et al., 2005b). Transfection studies have indicated that Mib1 directly interacts with and ubiquitinates the intracellular tails of Dl and Ser (Itoh et al., 2003; Chen and Casey Corliss, 2004; Lai et al., 2005; Le Borgne et al., 2005b). Although the importance of ligand endocytosis for Notch activation is well

Correspondence to François Schweisguth: fschweis@pasteur.fr

Abbreviations used in this paper: α4GT1, α1,4-*N*-acetylgalactosaminyltransferase-1; Brn, Brainiac; Cer, ceramide; Dl, Delta; Dlg, Discs large; E-Cad, E-cadherin; EGFR, EGF receptor; Egh, Egghead; GalNAc, *N*-acetylgalactosamine; GBM, GSL-binding motif; GlcNAc, *N*-acetylglucosamine; GSL, glycosphingolipid; HPA, *Helix pomatia* agglutinin; HPTLC, high performance thin layer chromatography; iDL, internalized Dl; Mib1; Mindbomb1; Neur, Neuralized; Ser, Serrate; SOP, sensory organ precursor; UAS, upstream activating sequence.

The Rockefeller University Press $30.00
J. Cell Biol. Vol. 188 No. 4 581–594
www.jcb.org/cgi/doi/10.1083/jcb.200907116

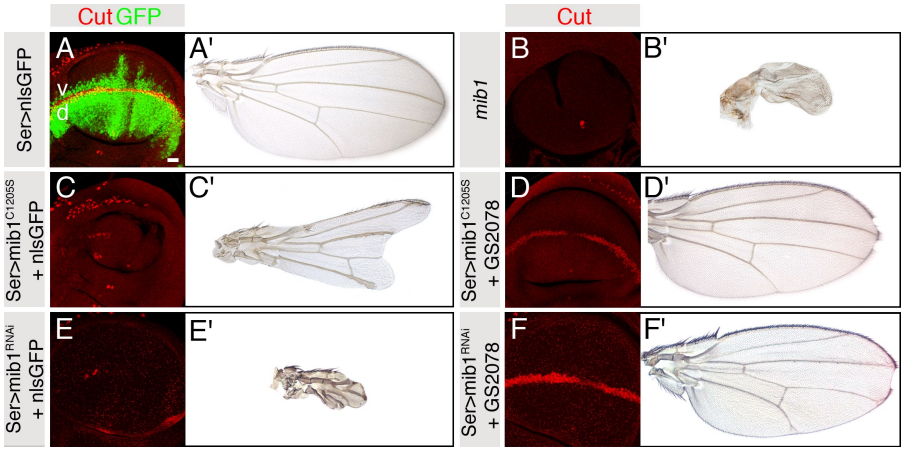

Figure 1. **Suppression of *mib1* by GS2078.** (A–F′) Genetic interactions between *mib1* and GS2078 were studied in third instar wing imaginal discs (A, B, C, D, E, and F) and in adult wings (A′, B′, C′, D′, E′, and F′). (A) The pattern of Ser-Gal4 expression was visualized using nlsGFP (green), and wing margin cells were identified using Cut (red). (A and A′) Wild-type control *UAS-nlsGFP/+; Ser-Gal4 tub-Gal80^{ts}/+* flies (Ser > nlsGFP) expressed nuclear GFP under the control of Ser driver in dorsal (d) cells as well as in some ventral (v) cells. Notch activation along the dorso–ventral boundary results in Cut expression at the wing margin. (B and B′) Trans-heterozygous *mib1^{2}/mib1^{3}* mutant disc and wing. Defective wing margin formation and wing pouch growth (B) result in a strong wing loss phenotype (B′). (C and C′) Expression of Mib1^{C1205S} in *UAS-nls-GFP/UAS-mib1^{C1205S}; Ser-Gal4 tub-Gal80^{ts}/+* flies (Ser > mib1^{C1205S} + nlsGFP) led to defective wing margin specification and reduced growth of the pouch. (D and D′) GS2078 suppressed the Mib1^{C1205S}-induced phenotype in *UAS-mib1^{C1205S}/+; Ser-Gal4 tub-Gal80^{ts}/GS2078* flies (Ser > mib1^{C1205S} + GS2078). Cut expression at the wing margin and wing pouch growth were significantly rescued. (E and E′) Down-regulation of *mib1* expression in *UAS-nlsGFP/+; Ser-Gal4 tub-Gal80^{ts} UAS-mib1^{RNAi}/+* flies (Ser > mib1^{RNAi} + nlsGFP) gave a *mib1* partial loss of function phenotype (compare with B and B′). (F and F′) GS2078 suppressed the hypomorphic *mib1* phenotype in *Ser-Gal4 tub-Gal80^{ts}UAS-mib1^{RNAi} GS2078/GS2078* flies (Ser > mib1^{RNAi} + GS2078). Cut expression at the wing margin and tissue growth were largely restored. Bar, 10 µm.

established, important questions remain. Indeed, it is not clear how ligand ubiquitination and endocytosis control receptor activation (D'Souza et al., 2008). Also, the steps at which Mib1 act during Notch ligand endocytosis and the factors, proteins, and lipids that contribute to this activity of Mib1 are largely not known.

In this study, we identify and characterize the *α1,4-N-acetylgalactosaminyltransferase1* (*α4GT1*) gene as a gain of function suppressor of *mib1* in *Drosophila*. Our genetic and biochemical analysis of *α4GT1* function indicates that specific changes in glycosphingolipid (GSL) composition can rescue the defects in Dl and Ser trafficking and signaling seen upon inhibition of *mib1* activity, thereby establishing a new functional link between GSLs and Notch signaling.

Results

Genetic identification of a dominant suppressor of *mib1*

To gain novel insights into the role and regulation of Notch ligand trafficking, we performed a genetic modifier screen for gain of function suppressors of a dominant-negative form of Mib1 (unpublished data). This mutant form of Mib1, Mib1^{C1205S}, was engineered by mutating a highly conserved amino acid of the catalytic C-terminal ring finger shown to disrupt Mib function in zebrafish (Itoh et al., 2003; Bardin and Schweisguth, 2006; Zhang et al., 2007). Conditional overexpression of Mib1^{C1205S} in wing imaginal discs inhibited Notch signaling as revealed by the loss of Cut and Wingless expression at the wing margin (Fig. 1, A and C; and not depicted) and by the nicks seen in adult fly wings (Fig. 1, A′ and C′). These phenotypes are similar to, albeit less severe than, the *mib1* mutant phenotypes (Fig. 1, B and B′). These phenotypes were suppressed by the expression of wild-type Mib1 (unpublished data), indicating that Mib1^{C1205S} interferes in a dominant-negative manner with the activity of endogenous Mib1.

A genetic screen for gain of function suppressors of the wing phenotype induced by Mib1^{C1205S} was performed using a collection of 4,000 Gene Search fly lines (unpublished data), each carrying a single, randomly inserted P-element with upstream activating sequences (UASs) at both ends (Toba et al., 1999). In this screen, UAS sequences were used to activate the transcription of endogenous genes located next to the Gene Search element using a *Ser*-GAL4 driver. This screen identified the GS2078 element as a strong suppressor of the wing phenotypes associated with Mib1^{C1205S} expression (Fig. 1, D and D′).

RNAi-mediated knockdown of *mib1* activity in wing imaginal discs using *Ser*-GAL4 produces a wing phenotype similar in strength to the one seen with Mib1^{C1205S} (Fig. 1, E and E′). The GS2078 element efficiently suppressed this partial loss of *mib1* function phenotype (Fig. 1, E–F′). It also reduced the penetrance of a wing nick phenotype seen in an hypomorphic heteroallelic combination of *mib1* mutant alleles (Fig. 2, H and I). However, it did not suppress the *mib1*-null mutant phenotype (Fig. 2, J–L). These genetic data indicate that the GS2078 element acts as a dominant suppressor of *mib1*.

The *α4GT1* gene is a gain of function suppressor of *mib1*

The GS2078 element is inserted 5′ to the *CG3542* and *α1,4-N-acetylgalactosyltransferase 1* (*α4GT1*) genes (Fig. 2 A) and may therefore direct the overexpression of both genes. However, several lines of evidence demonstrate that overexpression of *α4GT1* is responsible for the effect of GS2078. First, the EP797 element that directs the expression of the *α4GT1* gene (Protzer et al., 2009) suppressed the Mib1^{C1205S}-induced wing phenotypes (unpublished data). Second, overexpression of *α4GT1* using a UAS-cDNA construct also suppressed the Mib1^{C1205S}-induced defects (Fig. 2 C). Third, RNAi-mediated inactivation of the *α4GT1* gene blocked suppression by GS2078 (Fig. 2, E and F), indicating that overexpression of endogenous *α4GT1* is required to suppress the Mib1^{C1205S}-induced wing phenotypes.

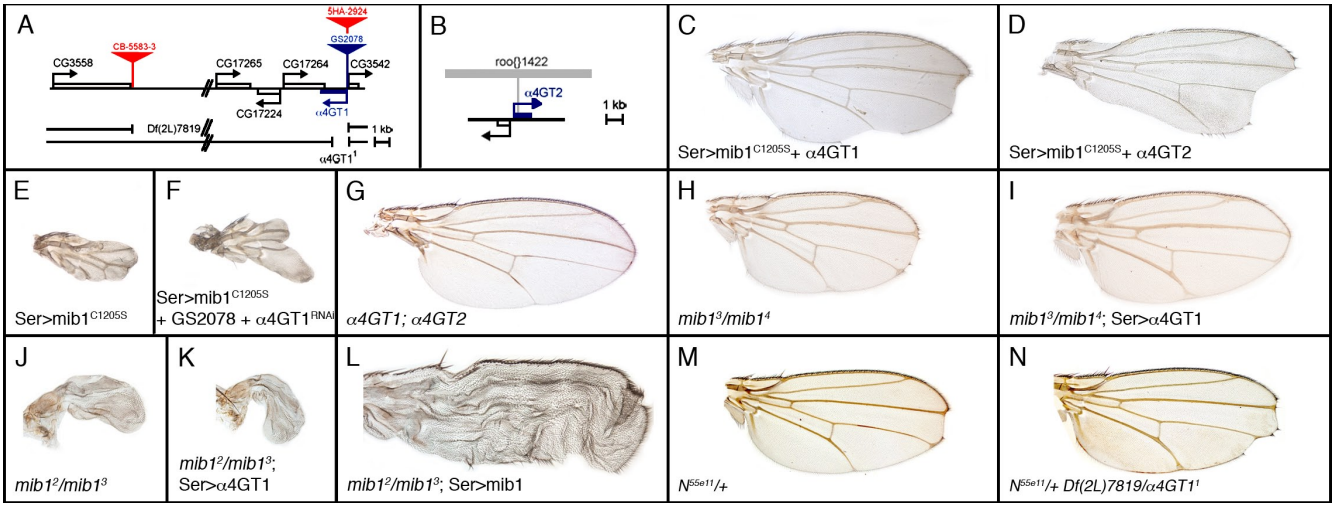

Figure 2. ***α4GT1* is a gain of function suppressor of *mib1*.** (A) Molecular map showing that the GS2078 P-element (blue) is inserted between and upstream of the *α4GT1* and *CG3542* genes. The breakpoints of the *Df(2L)7819* and of the small $\alpha4GT1^1$ deletions are indicated. *Df(2L)7819* deletes 24 kb of genomic DNA located between the 5HA-2924 and CB-5583-3 P-elements (red). It deletes the *α4GT1*, *CG17264*, *CG17224*, and *CG17265* genes and also partially deletes the *CG3542* gene. The $\alpha4GT1^1$ allele is a 1,201-nucleotide-long deletion that removes the sequence encoding the first 286 amino acids of the α4GT1 protein. Bar, 1 kb. (B) Molecular map of the *α4GT2* locus. The position of the roo 1,422 element disrupting the *α4GT2* open reading frame (red; transcript is in blue) in the $\alpha4GT2^1$ mutant allele is indicated. (C and D) Expression of α4GT1 in *UAS-mib1*^{C1205S}*/+; Ser-Gal4 tub-Gal80*^{ts}*/ UAS-α4GT1* flies (Ser > mib1^{RNAi} + α4GT1; C) and α4GT2 in *UAS-mib1*^{C1205S}*/+; Ser-Gal4 tub-Gal80*^{ts}*/UAS-α4GT2* flies (Ser > mib1^{RNAi} + α4GT2; D) suppressed the Mib1^{C1205S}-induced wing phenotypes. (E and F) RNAi-mediated down-regulation of *α4GT1* blocked suppression by GS2078 of the Mib1^{C1205S}-induced wing phenotype in *UAS-mib1*^{C1205S}*; Ser-Gal4 tub-Gal80*^{ts}*/GS2078; UAS-α4GT1*^{RNAi}*/+* (Ser > mib1^{C1205S} + GS2078 + α4GT1^{RNAi}; F). Note that the Ser > mib1^{C1205S} wing phenotype (E) is stronger than the one shown in Fig. 1 C′. This is because the x-linked mib1^{C1205S} transgene is expressed at higher levels in males (E and F) than in females (Fig. 1 C′). (G) $\alpha4GT1^1$*/Df(2L)7819*; $\alpha4GT2^1$ double-mutant flies have no detectable phenotype (compare with Fig. 1 A′). (H–L) Expression of *α4GT1* suppressed the hypomorphic *mib1* wing nick phenotype. (H and I) GS2078 lowered the penetrance of the hypomorphic $mib1^3$/$mib1^4$ wing nick phenotype: 11% (*n* = 194) of the $mib1^3$/$mib1^4$ wings exhibited nicks (H), whereas only 1% (*n* = 202) of *Ser-Gal4 tub-Gal80*^{ts}*/GS2078*; $mib1^3$/$mib1^4$ wings had nicks (I). In contrast, expression of *α4GT1* did not suppress the *mib1*-null phenotype. (J–L) The wing phenotype of $mib1^2$/$mib1^3$ flies (J) was rescued by the expression of *mib1* (L) but was not modified by the expression of *α4GT1* in *Ser-Gal4 tub-Gal80*^{ts}*/GS2078*; $mib1^3$/$mib1^4$ flies (K). (M and N) Loss of *α4GT1* function enhances the severity and penetrance of the haploinsufficient wing *Notch* phenotype: 19% (*n* = 16; 25°C) and 15% (*n* = 20; 29°C) of the N^{55e11} heterozygous flies show a small wing nick, whereas 66% (*n* = 132; 25°C) and 100% (*n* = 26; 29°C) exhibit nicks of increased size in the complete absence of *α4GT1* activity. Double-heterozygous *Notch α4GT1* flies were similar to N^{55e11} heterozygous flies in severity and penetrance. N^{55e11}/+; $\alpha4GT1^1$/+: 32% (*n* = 125) and N^{55e11}/+; *Df(2L)7819*/+: 28% (*n* = 96) at 25°C.

Therefore, we conclude that *α4GT1* overexpression is sufficient to suppress the Mib1^{C1205S}-induced defects and necessary for their suppression by GS2078. Together, our data identify the *α4GT1* gene as a gain of function suppressor of *mib1*.

α4GT1 is a nonessential *Notch* enhancer gene

The *α4GT1* gene encodes a ubiquitously expressed enzyme predicted to regulate GSL biosynthesis (Chen et al., 2007; Protzer et al., 2009). To investigate the role of the *α4GT1* gene in Notch signaling, we generated two molecularly null mutant alleles: the $\alpha4GT1^1$ allele deletes the first 286 amino acids of the α4GT1 protein, and the $\alpha4GT1^2$ allele carries a nonsense mutation at K131. We also generated a small molecularly mapped deletion, Df(2L)7819, that removes the *α4GT1* gene together with four additional predicted genes (Fig. 2 A). Flies transheterozygous for $\alpha4GT1^1$, $\alpha4GT1^2$, and/or Df(2L)7819 are viable and fertile, indicating that the *α4GT1* is a nonessential gene (Protzer et al., 2009; unpublished data). However, a complete loss of *α4GT1* activity significantly enhanced the haploinsufficient *Notch* mutant wing phenotype in both severity and penetrance (Fig. 2, M and N). This indicates that *α4GT1* plays a positive role in Notch signaling that can only be seen upon reduced Notch receptor activation.

Because the *Drosophila* genome encodes a second *α4GT* gene, *α4GT2* (Chen et al., 2007), which also behaved as a gain of function suppressor of Mib1^{C1205S} (Fig. 2 D), we tested whether *α4GT2* acts redundantly with *α4GT1*. We identified an *α4GT2* mutant allele, $\alpha4GT2^1$, with a roo{}1,422 element disrupting the *α4GT2* open reading frame (see Materials and methods; Fig. 2 B), generated *α4GT1 α4GT2* double-mutant flies, and found that these flies are phenotypically normal (Fig. 2 G). We conclude that the activities of the *α4GT1* and *α4GT2* genes are not strictly required for Notch signaling. Additionally, overexpression of *α4GT1* did not result in morphogically visible phenotypes (see Fig. 6 C and not depicted). Thus, *α4GT1* and possibly *α4GT2* play a nonessential modulatory role in Notch signaling.

α4GT1 overexpression suppressed *mib1*-dependent localization defects of Dl and Ser

To gain insight into the role of *α4GT1* in *mib1*-dependent signaling, we first investigated whether Mib1^{C1205S} perturbed the distribution of Dl and Ser in wing disc epithelial cells. In wild-type cells, Dl and Ser were detected into intracellular dots corresponding to endocytic vesicles and at the cortex where they colocalized with Patj, Crumbs, and E-cadherin (E-Cad;

Fig. 3, A–B″; and Fig. S1) and Notch (Fig. S2; Sasaki et al., 2007) apical to Discs large (Dlg; Fig. 3, G–G‴). Expression of Mib1^{C1205S} resulted in the accumulation of Dl and Ser in large apical dots (Fig. 3, C–D″ and H–H‴; and Figs. S1 and S2), whereas localization of Patj, Crumbs, and E-Cad were unchanged (Fig. S1). Cell surface staining experiments using antibodies directed against the extracellular domains of Dl and Ser indicated that Dl and Ser accumulated at the apical plasma membrane in Mib1^{C1205S}-expressing cells (Fig. S3). Dl and Ser colocalized with a YFP-tagged version of Mib1^{C1205S} (Fig. 3, H–H‴). This accumulation of Mib1^{C1205S} into dots did not depend on Dl and Ser (Fig. S2). Of note, these defects in Dl and Ser distribution differ from those seen in *mib1* mutant cells. Ser accumulated uniformly at the apical membrane in the absence of Mib1, whereas Dl localization remains unaffected (Fig. S2; Itoh et al., 2003; Lai et al., 2005; Le Borgne et al., 2005b). Furthermore, we noticed that Notch coaccumulated with Dl and/or Ser in Mib1^{C1205S}-expressing and *mib1* mutant cells (Fig. S2, C–H″). The accumulation of Notch into dots in Mib1^{C1205S}-expressing cells required the presence of Dl and Ser (Fig. S2, K–L″), indicating that this defective accumulation of Notch is a secondary consequence from the *mib1* defects in Dl and Ser accumulation. Together, these data suggest that Mib1^{C1205S} specifically altered the distribution of Dl and Ser by directly interacting with Dl and Ser and interfering with their endocytosis.

We then tested whether *α4GT1* overexpression suppressed the defects in Dl and Ser accumulation induced by Mib1^{C1205S}. The localization of Dl and Ser in cells expressing both dominant-negative Mib1 and α4GT1 was very similar to the one observed in wild-type cells (Fig. 3, E–F″ and I–I‴; Figs. S2 and S3). Thus, *α4GT1* suppressed the defects resulting from dominant-negative Mib1.

A similar suppression was observed in a context of partial loss of endogenous *mib1* activity. Cells with reduced *mib1* activity exhibited increased levels of Ser at the apical membrane (Fig. 4, A–D). This defect was suppressed by expression of *α4GT1* (Fig. 4, E–F). We conclude that expression of *α4GT1* rescued defects in Dl and Ser distribution caused by either dominant-negative Mib1 or reduced Mib1 activity.

α4GT1 overexpression restored endocytosis of Dl

We then investigated the basis of this suppression by *α4GT1*. We hypothesized that inhibition of Mib1 activity resulted in endocytosis defects and that *α4GT1* expression restored the endocytosis of the Notch ligands. The endocytosis of Dl was monitored in wing imaginal discs using an antibody uptake assay. In wild-type discs, internalized Dl (iDl) was detected in all cells expressing Dl (Fig. 5, A–B′). Expression of Mib1^{C1205S} in dorsal cells using Ser-GAL4 strongly inhibited Dl endocytosis (Fig. 5, C–D′), and overexpression of α4GT1 in these cells restored endocytosis of Dl (Fig. 5, E–F′).

We further investigated the role of *α4GT1* in regulating the Neur-dependent endocytosis of Dl in the pupal thorax (Le Borgne and Schweisguth, 2003). First, we found that the GS2078 element also suppressed the bristle phenotype that resulted from a partial loss of *neur* activity by RNAi (Fig. 6, I and K), the inhibition of Neur by Tom (Fig. 6, E and G; Bardin and Schweisguth, 2006), and the inhibition of Neur by dominant-negative Neur^{C701S} (the C701S mutation of Neur affects the same conserved amino acid of the RING finger as the C1205S mutation of Mib1; not depicted). Therefore, we conclude that *α4GT1* can positively regulate both Neur- and Mib1-dependent signaling events. We then monitored the endocytosis of Dl in sensory organ precursor (SOP) cells using an antibody uptake assay. Expression of *α4GT1* restored the endocytosis of Dl in SOPs in all experimental conditions of reduced and/or inhibited Neur activity (Fig. 6, E–L′; and not depicted). However, the loss of *α4GT1* and *α4GT2* activities had no detectable effect on the endocytosis of Dl in SOPs (unpublished data). The positive effect of α4GT1 expression on endocytosis may be cargo dependent because no major change in FM4-64 uptake was seen in cells overexpressing *α4GT1* (unpublished data).

α4GT1 regulates GSL biosynthesis

α4GT1 has been shown to catalyze the in vitro addition of an *N*-acetylgalactosamine (GalNAc) from a UDP-GalNAc donor to an α-GalNAc acceptor through an α1,4 linkage. In particular, α4GT1 efficiently transfered GalNAc to one of the major *Drosophila* GSLs, N4 or GalNAc-β1-4–*N*-acetylglucosamine(GlcNAc)–β1-3Manβ1-4Glcβ1-1-ceramide (Cer; Fig. 7 A; Chen et al., 2007; Stolz et al., 2008). GSLs are key components of the outer leaflet of the plasma membrane that have been proposed to regulate the formation of raftlike assemblies (Degroote et al., 2004; Sillence, 2007). GSLs are synthesized in the Golgi apparatus by Golgi-localized glycosyltransferases. In *Drosophila*, GSLs consist primarily of a Glcβ1-Cer core (GlcCer or N1) that can be elongated by the Egghead (Egh) GDP-mannose/βGlc β1,4-mannosyltransferase to form Manβ1-4Glcβ1-Cer (N2; Wandall et al., 2003) and by the Brainiac (Brn) UDP-GlcNAc/βMan β1,3-GlcNAc transferase that adds GlcNAc to form GlcNAc-β1-3Manβ1-4Glcβ1-Cer (N3; Fig. 7 A; Müller et al., 2002; Wandall et al., 2005). The latter can be further extended by a β1,4-*N*-acetylgalactosyltransferase, β4-GalNAc-TA or β4-GalNAc-TB, to form N4, the predicted α4GT1 substrate (Haines and Irvine, 2005; Chen et al., 2007; Stolz et al., 2008).

To test whether α4GT1 acts in vivo as an *N*-acetylgalactosamine transferase for GSLs, we first examined the effect of both loss and gain of *α4GT1* activity on the levels of terminal GalNAc at the surface of imaginal cells using the *Helix pomatia* agglutinin (HPA) lectin. This lectin selectively recognizes terminal α-GalNAc, present in N5, from other hexosyl, including the β-GalNAc of N4 (Sanchez et al., 2006; Iskratsch et al., 2009). We find that HPA cell surface staining was strongly reduced in clones of *α4GT1* mutant cells, demonstrating that α4GT1 is active in imaginal cells (Fig. 7, B and B′). Conversely, overexpression of α4GT1 in clones of imaginal cells resulted in strong HPA cell surface binding (Fig. 7, C and C′), suggesting that α4GT1 is a limiting enzyme in this tissue. These data indicate that α4GT1 catalyzes the addition of GalNAc to a detergent-sensitive substrate present at the cell surface.

Next, we biochemically characterized the role of α4GT1 in GSL biosynthesis by studying the chromatographic mobility

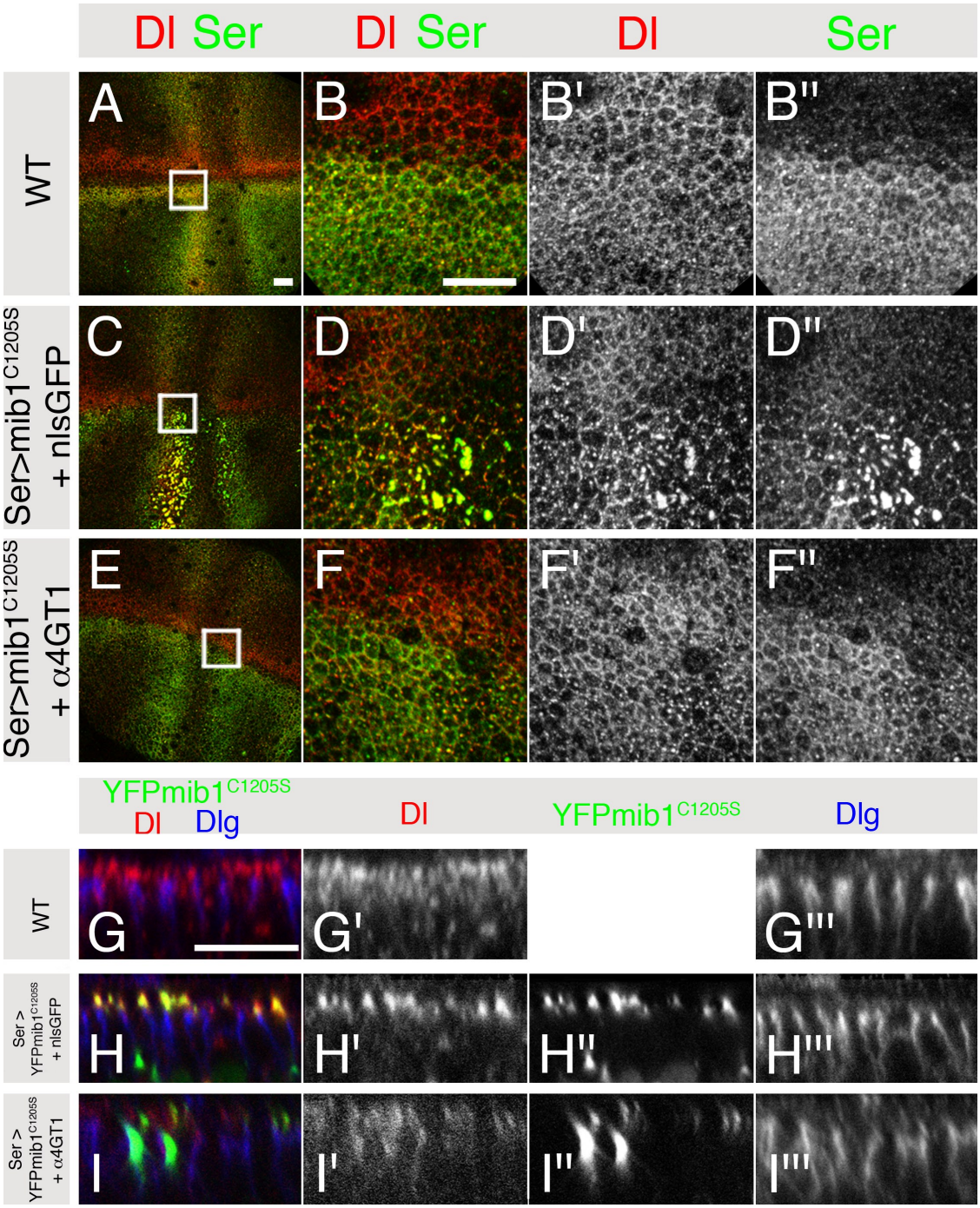

Figure 3. **α4GT1 rescued *mib1*^{C1205S} defects in Dl and Ser distribution.** Ser (green), Dl (red), YFP/mib1^{C1205S} (green), and Dlg (blue) distribution were analyzed in wing imaginal discs. (A–I‴) The following genotypes were studied: wild-type (WT; A–B″ and G–G‴), *UAS-nlsGFP/UAS-mib1*^{C1205S}*; Ser-Gal4 tub-Gal80*^{ts}*/+* (Ser > mib1^{C1205S} + nlsGFP; C–D″), *UAS-nlsGFP/UAS-YFPmib1*^{C1205S}*; Ser-Gal4 tub-Gal80*^{ts}*/+* (Ser > YFPmib1^{C1205S} + nlsGFP; H–H‴), *UAS-mib1*^{C1205S}*/+; Ser-Gal4 tub-Gal80*^{ts}*/GS2078* (Ser > mib1^{C1205S} + α4GT1; E–F″), and *UAS-YFPmib1*^{C1205S}*/+; Ser-Gal4 tub-Gal80*^{ts}*/GS2078* (Ser > YFPmib1^{C1205S} + α4GT1; I–I‴). Because Dl and Ser have distinct expression patterns (A), we focused our analysis to a dorsal region located near the margin where cells coexpress Dl and Ser. (B–F″) High magnification views of the areas boxed in A–E are shown. (G–I‴) Z-section views are shown. (A–B″ and G–G‴) In wild-type cells, Dl (B′ and G′) and Ser (B″) colocalized at the apical cortex, apical to Dlg (G‴). (C–D″ and H–H‴) Expression of Mib1^{C1205S} (C–D″) or YFPmib1^{C1205S} (H–H‴) led to the accumulation of Dl (D′, H′) and Ser (D″) into dots at the apical cortex, apical to Dlg (H‴). (E–F″ and I–I‴) Coexpression of α4GT1 with Mib1^{C1205S} (E–F″) or YFPmib1^{C1205S} (I–I‴) did not significantly change the distribution of Dl (F′ and I′) and Ser (F″) compared with wild-type controls. Bars, 10 µm.

of GSLs extracted from wild-type and mutant larvae. As described previously (Wandall et al., 2005; Chen et al., 2007; Stolz et al., 2008), five main GSL species were consistently detected (Fig. 7 D). These species were identified as Cer mono-, di-, tri-, tetra-, and pentahexoside and referred to as N1, N2, N3, N4, and N5, respectively, based on their mobility relative to standard GSLs. Extracts prepared from *α4GT1 α4GT2* double mutants exhibited an accumulation of N4 and a loss of N5,

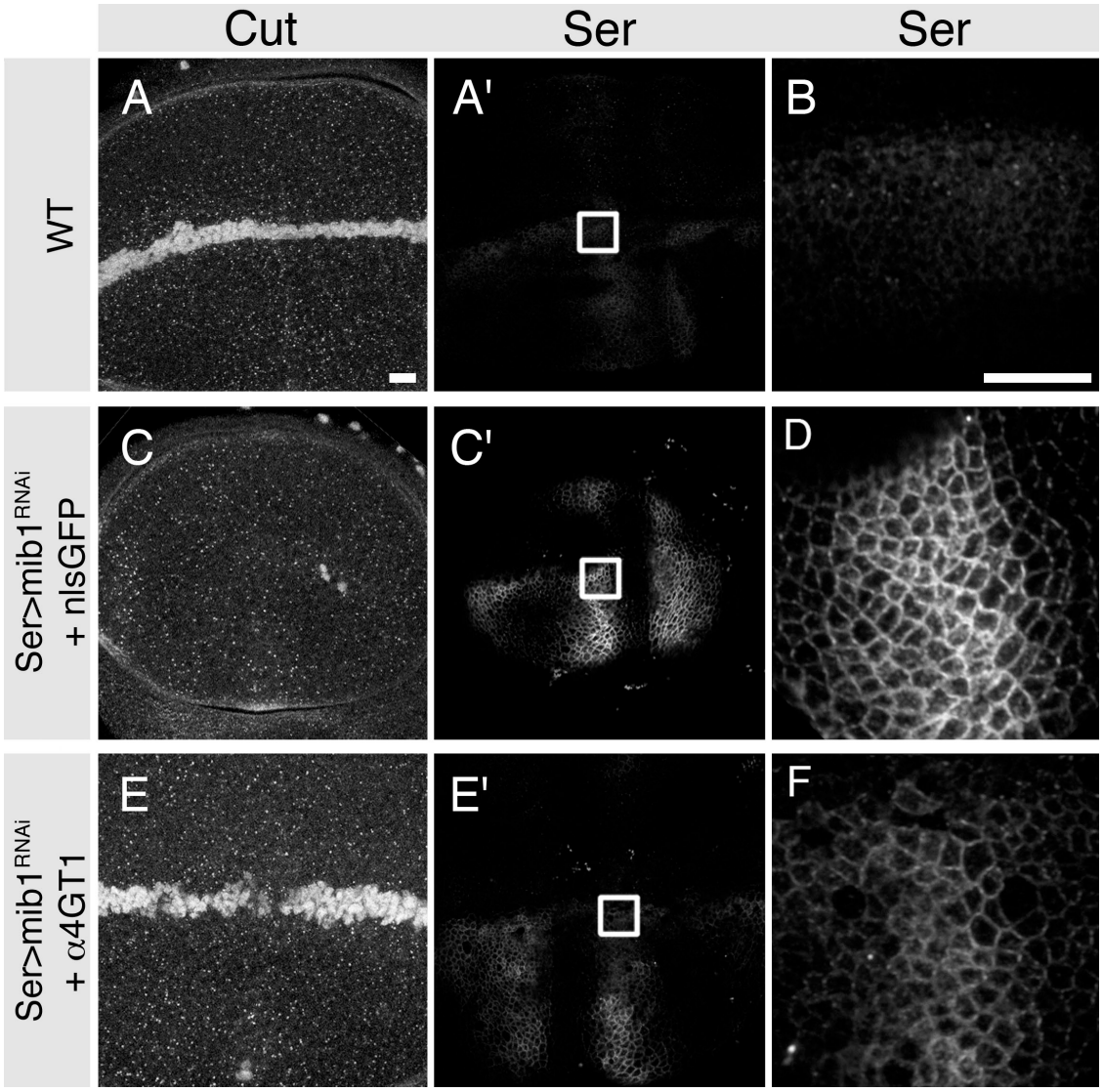

Figure 4. **α4GT1 rescued loss of *mib1* defects in Ser accumulation.** (A–F) The accumulation of Ser at the apical cortex of the cells and wing margin formation (using Cut as a marker) were examined in wild-type (WT; A–B), *UAS-nlsGFP/+; Ser-Gal4 tub-Gal80^{ts}UAS-mib1^{RNAi}/+* (Ser > mib1^{RNAi} + nlsGFP; C–D), and *Ser-Gal4 tub-Gal80^{ts}UAS-mib1^{RNAi}/GS2078* (Ser > mib1^{RNAi} + α4GT1; E–F) wing imaginal cells. High magnification views of the areas boxed in A′, C′, and E′ are shown in B, D, and F, respectively. (A′, B, C′, D, E′, and F) Single apical sections of stacks acquired using parameters adjusted to the high intensity signals measured in D are shown. These settings account for the low Ser signal in B. (A–B) Wild-type controls are shown. (A) Wing margin cells are specified as revealed by Cut expression along the dorsal–ventral boundary. (B) Low levels of Ser were detected at apical sections (fluorescence signal intensity = 1 ± 0.2 arbitrary units; $n = 3$). (C–D) RNAi-mediated inactivation of *mib1* resulted in increased Ser levels (D; fluorescence signal intensity = 16 ± 2.5; $n = 3$) and loss of wing margin (C). (E–F) Overexpression of *α4GT1* rescued the *mib1^{RNAi}* defects in Ser accumulation (F; fluorescence signal intensity = 3.4 ± 0.5; $n = 3$) and restored wing margin formation and pouch growth (E). Our quantification clearly indicates that the level of apical Ser was increased upon reduction of Mib1 activity in *mib1* RNAi cells and that expression of α4GT1 counteracts this effect. Bars, 10 µm.

indicating that α4GT1 and/or α4GT2 is required in vivo to synthesize N5 from N4 as previously proposed (Wandall et al., 2005; Chen et al., 2007; Stolz et al., 2008). Conversely, overexpression of α4GT1 resulted in a loss of N4 and an accumulation of N5 (Fig. 7 D), further indicating that α4GT1 is a limiting enzyme. As previously reported, N1 and N2 accumulated in *egh* and *brn* mutants, respectively, whereas N4 and N5 were not detected. Overexpression of α4GT1 in *egh* and *brn* mutant larvae did not significantly change the composition in GSLs of these mutants (Fig. 7 D), which is consistent with Egh and Brn being required to produce the N4 substrate of α4GT1. Together, these data indicate that α4GT1 modifies N4 to form N5.

GSL modification by *α4GT1* is required to rescue *mib1* defects

The aforementioned data raise the possibility that loss of N4 and/or accumulation of N5 rescue inhibition of Dl and Ser endocytosis caused by dominant-negative versions or RNAi-mediated down-regulation of *mib1* and *neur*. To test whether GSL modification is necessary for this activity of α4GT1, we examined whether the suppression of Mib1 inhibition by α4GT1 required the presence of GSLs produced by Egh and Brn. We found that overexpression of α4GT1 did not suppress the *mib1* RNAi–mediated wing margin phenotypes in the absence of *egh* activity and that suppression by α4GT1 was significantly reduced in *brn*

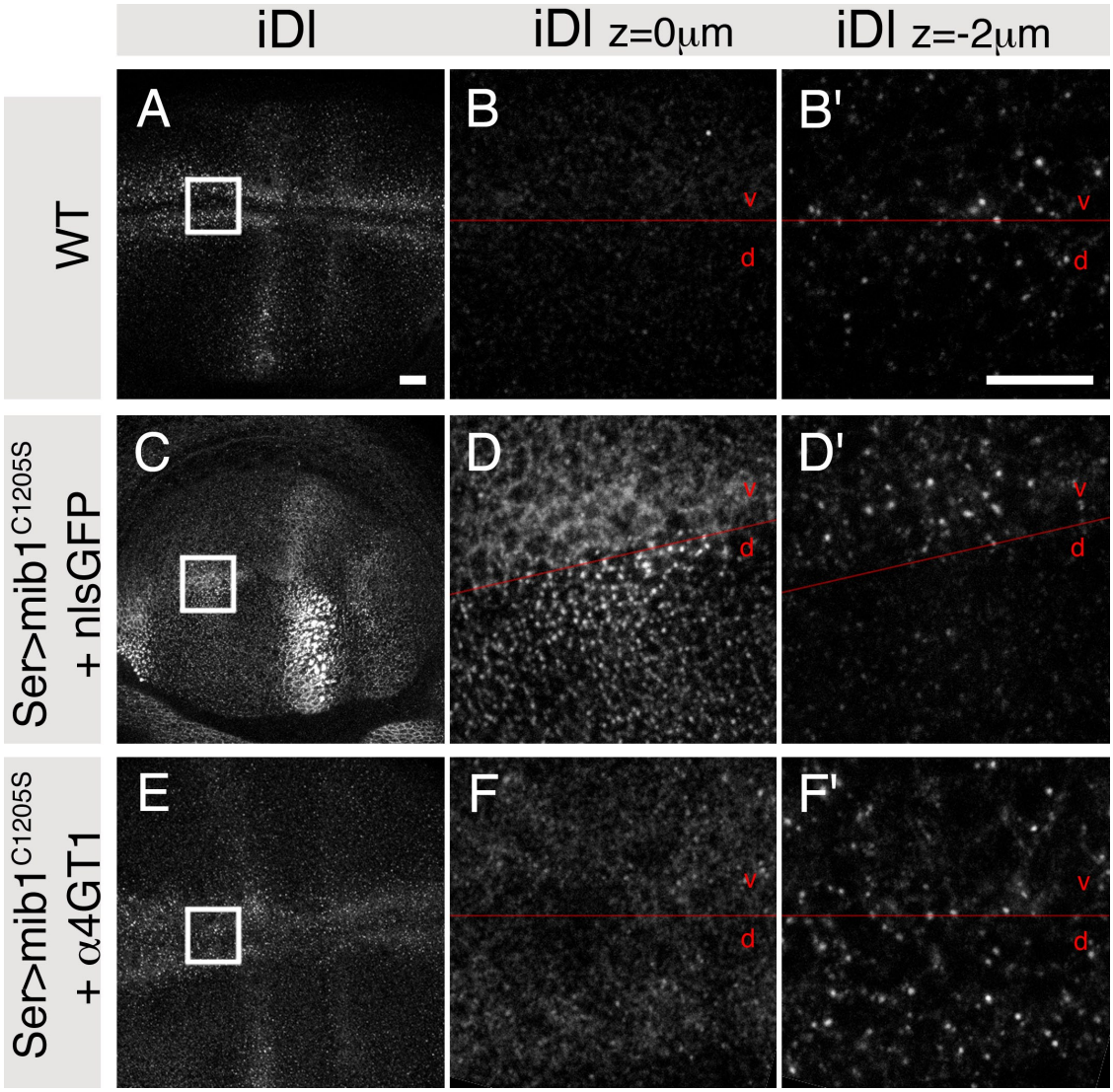

Figure 5. **α4GT1 rescued the endocytosis of Dl blocked by Mib1^{C1205S}.** The endocytosis of Dl was monitored in wing imaginal discs using an antibody uptake assay in wild-type (A–B′), *UAS-nlsGFP/UAS-mib1^{C1205S}; Ser-Gal4 tub-Gal80^{ts}/+* (Ser > mib1^{C1205S} + nlsGFP; C–D′), and *UAS-mib1^{C1205S}/+; Ser-Gal4 tub-Gal80^{ts}/GS2078* (Ser > mib1^{C1205S} + α4GT1; E–F′). The approximate position of the dorsal (d)–ventral (v) boundary is indicated in red. (A–B′) In wild-type discs, iDl was detected in subapical sections (B′) in both dorsal and ventral cells that express Dl (Fig. 3 A). (C–D′) Expression of Mib1^{C1205S} in dorsal cells using Ser-GAL4 inhibited the endocytosis of Dl (D′). In these cells, dots of Dl were only detected in apical sections (D). This staining is very similar to the one seen in cell surface staining experiments (Fig. S3), indicating that Mib1^{C1205S} inhibits the internalization of Dl. iDl was only seen in the ventral cells (D′) that express Mib1^{C1205S} later and at a lower level (Fig. 1 A). (E–F′) Expression of α4GT1 restored the endocytosis of Dl. (F′) iDl was detected in both ventral and dorsal cells. (F) Only weak cell surface staining was observed. High magnification views of boxed areas shown in A, C, and E are shown in B and B′, D and D′, and F and F′, respectively. Bar, 10 µm.

mutant discs (Fig. 7, E–M). These data support the notion that modification of N4 by α4GT1 is required to rescue a partial loss of *mib1* activity. Loss of N4 is not sufficient per se to rescue inhibition of Mib1 because the *mib1* RNAi–mediated wing margin phenotype is not suppressed in *egh* and *brn* mutants that do not accumulate N4 (Fig. 7 D). Alternatively, accumulation of N5 may compensate for a partial loss of Mib1 activity. Consistent with this interpretation, a Gene Search line inserted 2.5 kb 5′ to the β4-GalNAc-TA gene was also isolated as a dominant suppressor in our genetic screen, raising the possibility that increased N4 and/or N5 levels as a result of β4-GalNAc-TA overexpression also suppressed the Mib1^{C1205S}-induced defects. Whether accumulation of N5 is actually sufficient to rescue inhibition of Mib1 remains to be tested.

A conserved GSL-binding motif (GBM) in Dl and Ser

The aforementioned data raise the possibility that N5 positively regulates the endocytosis of Notch ligands, at least when the function of Mib1 is compromised. Various mechanisms, direct and indirect, could potentially underlie this positive regulation, including mechanisms involving a direct interaction between GSLs and the Notch ligands. As a first step to test this hypothesis, we searched for potential GBMs in the extracellular domain of Dl and Ser using an in silico approach (Mahfoud et al., 2002; Fantini et al., 2006). A putative GBM was predicted in the N2 domain of Dl and Ser (Fig. 8 A). This predicted GBM contains a conserved Trp residue flanked by turn-inducing and polar amino acid residues, suggesting that it could belong to a

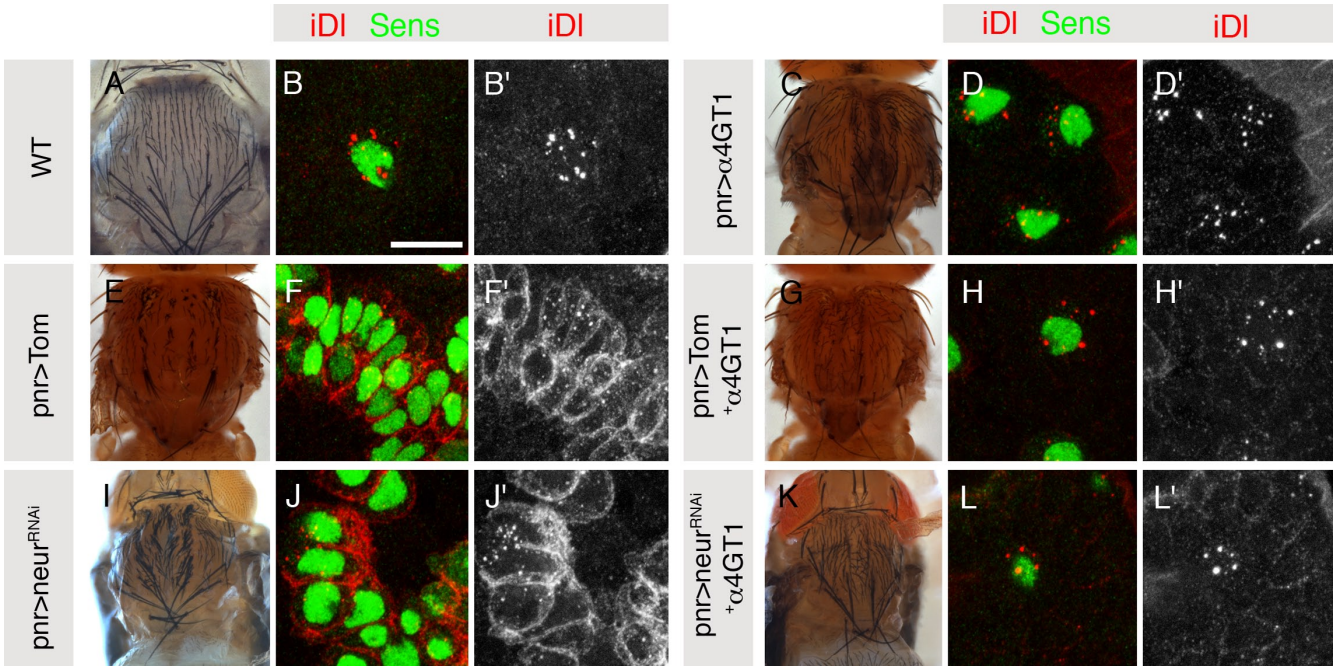

Figure 6. **α4GT1 restored the Neur-dependent endocytosis of Dl in SOPs.** (A–L′) The endocytosis of Dl (iDl in red) was monitored in SOPs (marked by Senseless [Sens] in green) using an antibody uptake assay in pupae of the following genotypes: wild-type (WT; A–B′); *GS2078/+; pnr-GAL4 tub-Gal80^{ts}/+* (pnr>α4GT1; C–D′); *UAS-Tom/+; pnr-GAL4 tub-Gal80^{ts}/+* (pnr > Tom; E–F′); *UAS-Tom/GS2078; pnr-GAL4 tub-Gal80^{ts}/+* (pnr > Tom + α4GT1; G–H′); *UAS-neur^{RNAi}/+; pnr-GAL4 tub-Gal80^{ts}* (pnr > neur^{RNAi}; I–J′); and *UAS-neur^{RNAi}/GS2078; pnr-GAL4 tub-Gal80^{ts}* (pnr > neur^{RNAi} + α4GT; K–L′). (A–D′) Expression of *α4GT1* did not detectably affect the endocytosis of Dl in SOPs (D and D′) and did not significantly change bristle density (C). (E–H′) Inhibition of Neur by Tom blocked Dl endocyosis (F and F′) and resulted in a very strong neurogenic phenotype (E) with too many SOPs being specified (F). Expression of *α4GT1* restored both Dl endocytosis (H and H′) and proper SOP specification (G and H). (I–J′) RNAi-mediated down-regulation of *neur* strongly inhibited Dl endocyosis (J and J′) and resulted in a strong neurogenic phenotype (I) with an excess of SOPs (J′). Expression of *α4GT1* restored both Dl endocytosis (H and H′) and suppressed the *neur* RNAi bristle phenotype (G and H). Bar, 10 µm.

solvent-exposed hairpin structure and, therefore, interact with the sugar head group via a CH-Pi stacking mechanism (Maresca et al., 2008). These structural features are typical of functional GBMs (Hebbar et al., 2008) and are conserved in vertebrate homologues of Dl and Ser (Fig. 8 A).

To test whether these predicted GBMs interact with GSLs, we first used the Langmuir film balance technique with synthetic peptides and GSLs purified from wild-type larvae. In these experiments, a lipid fraction enriched in GSLs was spread at the air–water interface where they readily formed a stable monolayer mimicking the extracellular leaflet of the plasma membrane. Under these conditions, an increase in the surface pressure of the monolayer upon injection of the peptide in the aqueous phase is indicative of insertion of the peptide in the glycolipid monolayer (Mahfoud et al., 2002; Fantini et al., 2006). Upon addition of the Ser and Dl GBM peptides, the surface pressure increased to reach a plateau value of 10.8 and 4.4 mN/m, respectively (Fig. 8 B). Replacing the Trp residue by Ala in both peptides abolished interaction, indicating that the Trp residue is essential for the interaction between GSLs and GBM peptides.

We next tested whether the N-terminal part of Ser, Ser[1–288], which includes the N1, N2, and DSL domains, interacts with GSLs in a GBM-dependent manner. Secreted wild-type and GBM mutant versions of Ser, Ser[1–288] and Ser[1–288]^{WA}, respectively, were produced in S2 cells and purified from the culture medium. Ser[1–288] and Ser[1–288]^{WA} interacted similarly with control phosphatidylethanolamine or a neutral lipid fraction prepared from *egh* mutant larvae (Fig. 8, C and D). In contrast, Ser[1–288] interacted more strongly with GSLs prepared from wild-type larvae than Ser[1–288]^{WA} (Fig. 8, C and D). We conclude that the N-terminal part of Ser interacts with GSLs and that this interaction depends on the W180 of the GBM.

To test the potential role of the N4 and N5 GSLs in this interaction, we studied the interaction of Ser[1–288] and Ser[1–288]^{WA} with GSLs prepared either from *α4GT1 α4GT2* double mutants, which are high in N4 but low in N5, or from larvae overexpressing *α4GT1*, which are low in N4 but high in N5. A stronger and specific interaction was upon increased N5 (and decreased N4) levels (Fig. 8 D, compare overexpression of *α4GT1* with wild type), whereas depletion in N5 (and accumulation of N4) had no effect (Fig. 8 D, compare *α4GT1 α4GT2* with wild type). We conclude that Ser interacts with GSLs via a conserved GBM and that this interaction is sensitive to the levels of N5 and/or N4. These in vitro data suggest that differences in N4 and/or N5 levels within the plasma membrane modulate the endocytosis of Dl and Ser via direct GSL–protein interaction.

Discussion

In this study, we identify *α4GT1* as a positive, nonessential regulator of Notch signaling in *Drosophila*. Expression of *α4GT1* suppressed the phenotypes associated with the inhibition or a

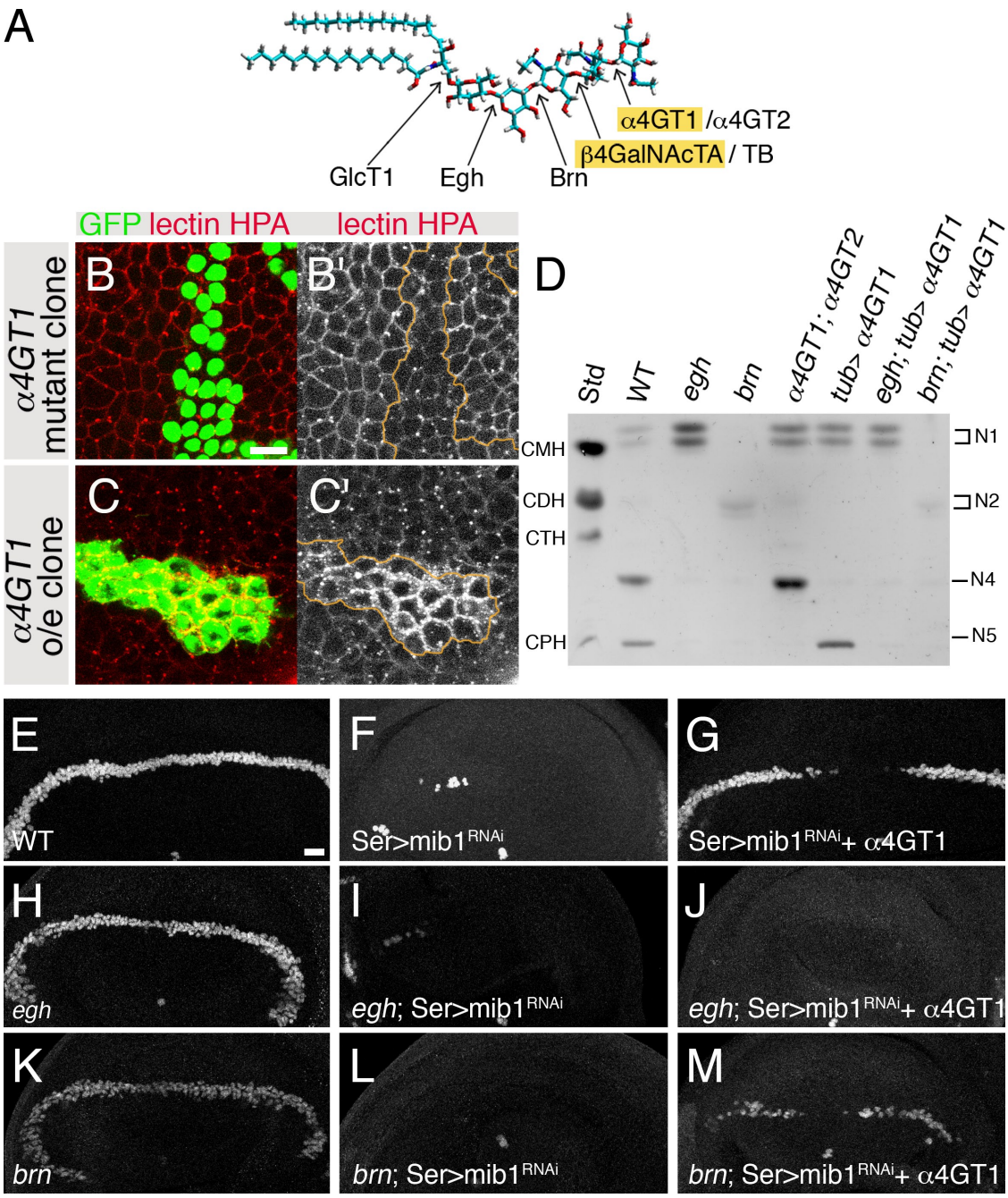

Figure 7. **Rescue of *mib1* inhibition by *α4GT1* depends on *egh* and *brn* activities.** (A) Molecular structure of GalNAc-α1-4-GalNAc-β1-4-GlcNAcβ-1-3Manβ1-4Glcβ1-1Cer or N5. The enzymes acting sequentially in the N5 biosynthetic pathway are indicated below (see Results). The two dominant suppressors identified in our screen are highlighted in yellow. (B–C') Analysis of α-GalNAc distribution in pupal notum epithelial cells using HPA (TRITC-HPA in red). HPA staining was strongly reduced in clones of *α4GT1* mutant cells (B and B'; mutant cells are marked by nuclear GFP in green), indicating that *α4GT1* is required for α-GalNAc localization at the cell surface. Overexpression (o/e) of *α4GT1* in clones (CD8-GFP in green) resulted in increased HPA staining, indicating that α4GT1 is a limiting enzyme for addition of α-GalNAc. (D) HPTLC analysis of GSLs purified from wild-type (WT) and mutant larvae. (lane 1) Standard GSLs: CMH, Cer monohexoside (GlcCer); CDH, Cer dihexoside (LacCer); CTH, Cer trihexoside (Gb3); and CPH, Cer pentahexoside (Forsmann glycolipid). The GSL species detected in larvae extracts (N1, N2, N4, and N5) were identified on the basis of their chromatographic mobility as compared with standard GSLs. (lane 2) Wild type. (lane 3) egh^{62D18}/Y. (lane 4) $brn^{l.6P6}$/Y. (lane 5) *α4GT1*^{1}*/Df(2L)7819; α4GT2*^{1}. (lane 6) Overexpression of *α4GT1* in wild-type larvae: *tub-GAL4/GS2078*. (lane 7) Overexpression of *α4GT1* in *egh* mutant larvae: egh^{62D18}*/Y; tub-GAL4/GS2078*. (lane 8) Overexpression of *α4GT1* in *brn* mutant larvae: $brn^{l.6P6}$*/Y; tub-GAL4/GS2078*. (E–M) Rescue of *mib1* inhibition by α4GT1 depends on *egh* and *brn* activities. Wing margin specification (marked by Cut) was examined in wild-type (E), Ser > mib1^{RNAi} + nlsGFP (F), Ser > mib1^{RNAi} + α4GT1 (G), egh^{62D18}/Y (H), egh^{62D18}/Y; Ser > mib1^{RNAi} + nlsGFP (I), egh^{62D18}/Y; Ser > mib1^{RNAi} + α4GT1 (J), $brn^{l.6P6}$/Y (K), $brn^{l.6P6}$/Y; Ser > mib1^{RNAi} + nlsGFP (L), and $brn^{l.6P6}$/Y; Ser > mib1^{RNAi} + α4GT1 (M) wing discs. Zygotic loss of *egh* and/or *brn* did not significantly alter the expression of Cut at the wing margin (E, H, and K) and did not enhance the Ser > mib1^{RNAi} phenotype (F, I, and L). In the absence of *egh* activity, α4GT1 expression failed to restore wing margin specification (J) as it did in wild-type discs (G). (M) Suppression by α4GT1 was strongly reduced in *brn* mutant discs. The partial suppression seen in *brn* mutants may result from maternally provided *brn* gene products. Alternatively, *egh* may have a *brn*-independent function in this tissue. Bars, 10 μm.

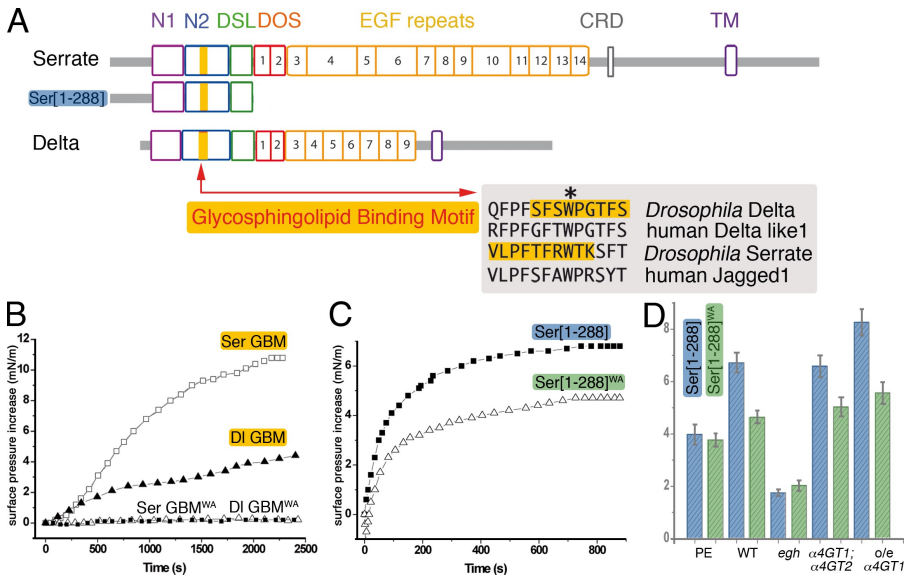

Figure 8. **Identification of a conserved GBM.** (A) Schematic representation of the structure of Dl and Ser (adapted from Parks et al., 2006). The domain structure of Ser[1–288] is also indicated. The potential GBM detected in the N2 domain of Dl and Ser appears in yellow. This GBM is conserved in mammals: the sequences of human Dl–like 1 and Jagged1 are aligned with the GBM of *Drosophila* Dl and Ser. The sequences of the synthetic peptides used in B and C are boxed in yellow. The Trp (W) residue shown in B required for interaction with GSLs is indicated with an asterisk. DSL, Dl/Ser/LAG-2; DOS, Dl- and OSM-11–like proteins; CRD, cysteine-rich domain; TM, transmembrane domain. (B) Analysis of GBM–GSL interactions. Synthetic peptides corresponding to the GBM of Ser and Dl interacted with total GSLs extracted from wild-type larvae. Interactions were quantitatively measured using the Langmuir film balance technique. The conserved Trp residue is essential for these interactions. The following peptides were studied: Ser GBM (open squares; VLPFTFRWTK), Ser GBM^{WA} (closed squares; VLPFTFRATK), Dl GBM (closed triangles; SFSWPGTFS), and Dl GBM^{WA} (open triangles; SFSAPGTFS). (C and D) Analysis of Ser–GSL interactions. Interactions of the Ser[1–288] (closed squares in C; blue bars in D) and Ser[1–288]W180A (open triangles in C; green bars in D) proteins secreted from S2 cells with phosphatidylethanolamine (PE) and total GSLs extracted from wild-type, *egh*, *α4GT1 α4GT2* double-mutant, and *tub-GAL4 UAS-α4GT1* (overexpressed *α4GT1*) larvae were quantitatively measured using the Langmuir film balance. The binding kinetics are shown in C, and the values of the maximal surface pressure increases are given in D. (D) Ser[1–288] and Ser[1–288]^{WA} similarly interacted with PE and neutral lipids prepared from *egh* mutant larvae. This indicates that the N-terminal part of Ser interacts in a GBM-independent manner with lipid monolayers in this assay. In contrast, Ser[1–288] interacted more strongly than Ser[1–288]^{WA} with total GSLs extracted from wild-type, *α4GT1 α4GT2* double-mutant, and *tub-GAL4 UAS-α4GT1* larvae, indicating that the N-terminal part of Ser interacts in a GBM-dependent manner with GLSs. Moreover, a stronger and GBM-dependent interaction correlated with high levels of N5 (and low levels of N4) in overexpressed *α4GT1* larvae. Error bars indicate SD (n = 3 experiments).

partial loss of *neur* and/or *mib1* activities in at least two developmental contexts. Conversely, the loss of *α4GT1* function enhanced a partial loss of *Notch* activity. Although the complete loss of *α4GT1* activity has no detectable phenotypic consequences, these genetic interactions indicate that α4GT1 plays a positive role in Notch signaling in *Drosophila*.

Several lines of evidence indicate that this function of α4GT1 involves a specific modification of GSLs. First, HPA lectin staining experiments showed that *α4GT1* is both necessary and sufficient for the addition of terminal α-GalNAc at the cell surface of imaginal cells. Second, chromatography analysis indicated that *α4GT1* is both necessary and sufficient for the biosynthesis of the N5 GSL from its N4 precursor. Third, suppression of the partial loss of function *mib1* phenotype by *α4GT1* required the activity of the glycosyltransferases Egh and Brn. Because extension of the Manβ1-4Glcβ1-Cer core by Egh and Brn produces a terminal lacdiNAc that, despite intensive analyses of glycoproteins (North et al., 2006), has only been found on GSLs (Seppo et al., 2000), we conclude that synthesis of N5 from its precursor N4 underlies the suppression of the *mib1*-dependent defects by *α4GT1*.

The in vivo functions of GSLs are not well understood (Degroote et al., 2004; Sillence, 2007). Several studies indicate that GSLs play a role in modulating the signaling activity of cell surface receptors. For instance, GSLs have been shown to negatively regulate the signaling activity of the EGF receptor (EGFR), and this negative regulation appears to involve a direct interaction between the EGFR and a specific GSL, GM3 (Yoon et al., 2006). Specific GSLs have also been implicated in caveolar endocytosis and β1-integrin signaling (Sharma et al., 2004; Singh et al., 2007). In *Drosophila*, genetic analyses have indicated that the activities of Egh and Brn are required for both epithelium integrity and planar transport of an EGFR ligand (Goode et al., 1996; Wandall et al., 2003; Pizette et al., 2009). The *egh* and *brn* genes have also been suggested to regulate neurogenesis in the early embryo (Goode et al., 1996). However, our analysis of the *brn* mutant phenotypes indicated that this developmental defect does not result from defective Notch signaling (unpublished data). The *Caenorhabditis elegans* homologues of *egh* and *brn*, *bre-4*, and *bre-5* act as suppressors of a gain of function allele of the Notch family receptor gene *lin-12* genes (Griffitts et al., 2005; Katic et al., 2005). Although the molecular basis underlying these genetic interactions is not known, *bre-5* was shown to act in a non–cell-autonomous manner, raising the possibility that GSLs modulate the signaling activity of the Lin-12 ligands. Although the *bre-4* and *bre-5* genes play a positive role in Lin-12 signaling in *C. elegans*, these two genes are not essential in *C. elegans* (Griffitts et al., 2005; Katic et al., 2005). This situation is very reminiscent of the nonessential modulatory role of *Drosophila α4GT1* uncovered in this study. Thus, GSLs appear to play a conserved modulatory role in Notch signaling. Of note, a nonessential role has also been proposed for phospholipids: mutations in the *Drosophila phosphocholine cytidylyltransferase 1* gene reduced phosphatidylcholine and increased phosphatidylinositol levels at the plasma membranes and enhanced Notch hypomorphic phenotypes (Weber et al., 2003).

What is the role of GSLs in Notch signaling? Our biochemical and genetic interaction experiments indicate that high N5 levels can compensate for reduced levels of Neur and/or

Mib1 activity. In several experimental situations, i.e., inhibition of Mib1 by dominant-negative Mib1 in wing imaginal cells, inhibition of Neur in notum cells by Tom or dominant-negative Neur, partial loss of *neur* activity in notum cells using RNAi, we observed that *α4GT1* expression restored normal levels of Dl endocytosis. Therefore, we propose that high levels of N5 positively regulate the endocytosis of Dl. However, this role of N5 has so far only been observed in sensitized contexts in which Dl endocytosis is inhibited. In particular, no increase in *neur*-dependent endocytosis of Dl was seen in SOPs overexpressing *α4GT1*. The restoration of proper Ser localization by α4GT1 in cells with reduced *mib1* activity very likely reflects a similar role of N5 on the endocytosis of Ser. The role proposed in this study for GSLs in Notch ligand endocytosis is entirely consistent with the nonautonomy observed for *bre-5* in *C. elegans* (Katic et al., 2005). It is also consistent with the localization of mammalian Dl–like 1 in detergent-resistant membranes that are enriched in cholesterol and sphingolipids (Heuss et al., 2008).

This in turn raises the question of how GSLs influence the endocytosis of Dl and Ser. A first possibility is that high levels of N5 GSLs have a general effect on endocytosis. However, this view is not supported by our observation that the uptake of FM4-64 did not appear significantly changed upon α4GT1 overexpression. A second possibility is that α4GT1 expression indirectly results in increased enzymatic activity of the E3 ubiquitin ligases Neur and Mib1. A third possibility is that changes in GSL composition of the plasma membrane modify the distribution and organization of lipids, thereby promoting the organization of specific nanodomains. Accordingly, α4GT1 expression could modify the distribution of specific cargoes, including Dl and Ser, at the plasma membrane. For instance, clustering of Dl and Ser within N5-containing nanodomains might facilitate their endocytosis, thus signaling activity. Consistent with this view, one proposed function of GSLs is to promote endocytosis (Sharma et al., 2004). This view is also supported by our identification of a conserved GBM present in both Dl and Ser that interacts in vitro with GSLs. Although the function of this GBM remains to be tested in vivo, we note that four different Alagille syndrome misense mutations in the human *Jagged1* gene map to the 10–amino acid sequence of the GBM (Crosnier et al., 1999; Röpke et al., 2003). Furthermore, the strength of the interaction between Ser and GSLs depends on N4 and/or N5 levels. Specifically, lipid monolayers enriched in N5 appeared to interact in vitro more strongly with the N-terminal extracellular domain of Ser in a GBM-dependent manner. Finally, we speculate that this role of GSLs in endocytosis cannot bypass the strict requirement for ubiquitination of the Notch ligands because expression of α4GT1 did not suppresss the *mib1*-null phenotype. Whether Dl and Ser interact in vivo with GSLs, either within the same cell or across the intercellular space of neighboring cells, and whether this interaction regulates the endocytosis and activity of Dl and Ser remain to be investigated. In summary, our study uncovers a novel regulatory but nonessential function of GSLs in *Drosophila* and establishes a new functional link between the E3 ubiquitin ligase–dependent endocytosis of Dl and Ser and specific GSLs.

Materials and methods

Flies

The GS2078 line was generated by the *Drosophila* Gene Search Project (http://gsdb.biol.metro-u.ac.jp/~dclust/index.html). We identified this Gene Search line in a screen for suppression of the wing phenotype induced by the expression of Mib1^{C1205S} in *Ser-GAL4 tub-GAL80^{ts} UAS-mib1^{C1205S}* flies. The *Ser-GAL4 tub-GAL80^{ts}* and *pnr-GAL4 tub-GAL80^{ts}* chrosomomes were obtained by recombining previously described transgenes and enhancer trap insertions (http://flybase.org/). *UAS-mib1^{C1205S}* flies were described previously (Le Borgne et al., 2005b). All crosses involving *Ser-GAL4 tub-GAL80^{ts}* and *pnr-GAL4 tub-GAL80^{ts}* were at 25°C, and the progeny was transfered at 28°C at the first/second instar larval stage to allow for postembryonic GAL4-dependent expression.

The Df(2L)7819 deletion was generated by FLP/FRT recombination as described previously (http://www.drosdel.org.uk/ddelements.html; Golic and Golic, 1996). It deletes the 23,984 nucleotide located between the P-elements 5HA-2924 and CB-5583-3. The structure of Df(2L)7819 was verified by PCR amplification of the recombined P-element. The *α4GT1^{1}* allele was generated by imprecise excision of the 5HA-2924 P-element. The breakpoints of the small deletion associated with this allele were determined by sequencing a PCR fragment amplified from genomic DNA prepared from *α4GT1^{1}/Df(2L)7819* flies.

The *α4GT1^{2}* allele was selected by the *Drosophila* Tilling project (Cooper et al., 2008), and the molecular lesion was verified by sequencing. The EP797 line was obtained from the Szeged Stock Center. The *α4GT2^{1}* allele was present in the strain sequenced by the *Drosophila* Genome Project. The presence of the roo element was verified by genomic PCR experiments.

mib1 mutant allleles were described previously (Le Borgne et al., 2005b). The *mib1^{2}/mib1^{3}* is a null trans-heterozygous combination, whereas the *mib1^{3}/mib1^{4}* represents a hypomorphic combination. The UAS-mib1^{RNAi} was obtained from the Vienna *Drosophila* RNAi Center (line ID27525). The UAS-neur^{RNAi} line was obtained from R. Ueda (National Institute of Genetics, Mishima, Japan; http://www.shigen.nig.ac.jp/fly/nigfly/index.jsp). The *egh^{62D18}* and *brn$^{l.6P6}$* mutations were described previously (Goode et al., 1996; Wandall et al., 2003). All other mutations and fly stocks used in this study are described in FlyBase (http://flybase.org/).

The following transgenes were produced in this study: UAS-α4GT1, UAS-α4GT2, UAS-YFPmib1^{C1205S}, and UAS-YFPneur^{C701S} (cloning details for these constructs are available upon request). Transgenic flies were generated via standard P-element transformation.

Mitotic clones were induced in first and second instar larvae using a 45-min heat shock at 36.5°C. *mib1^{2}* clones were generated in *hs-flp tub-Gal4 UAS-GFP;; FRT2A mib1^{2}/tub-Gal80 FRT2A* larvae. Clones of *Dl Ser* mutant cells expressing Mib1^{C1205S} were generated in *hs-flp tub-Gal4 UAS-GFP/UAS-mib1^{C1205S};; FRT82B Dl^{rev10} Ser^{Rx82}/tub-Gal80 FRT82B* larvae. Control clones were generated in *hs-flp tub-Gal4 UAS-GFP/UAS-mib1^{C1205S};; FRT82B/tub-Gal80 FRT82B* larvae. *α4GT1* clones were generated in *hs-flp tub-Gal4 UAS-GFP;; FRT40A Df(2L)7819/tub-Gal80 FRT40A* larvae. *α4GT1* overexpression clones were generated in *hs-flp; tub-Gal4 UAS-mCD8-GFP/GS2078; FRT82B/tub-Gal80 FRT82B*.

Immunostainings and endocytosis assays

Dissection and antibody staining were performed using standard procedures. The following antibodies were used: mouse anti-Cut (2B10 ascite; 1:500; Developmental Studies Hybridoma Bank [DSHB]), rat anti-Ser (1:1,000; provided by K. Irvine, Rutgers University, Piscataway, NJ; Papayannopoulos et al., 1998), mouse anti-Dl (C594.9B; 1:1,000; DSHB; Kooh et al., 1993), mouse anti-Notch (C458.2H; 1:1,000; DSHB; Fehon et al., 1991), rabbit anti-Patj (1:500; provided by K. Choi, Baylor College, Houston, TX; Bhat et al., 1999), rat anti–E-Cad2 (1:500; DSHB; Oda et al., 1994), rat anti-Crumbs (1:1,000; provided by U. Tepass, Toronto University, Toronto, Ontario, Canada; Tepass and Knust, 1993), guinea pig anti-Senseless (1:2,000; provided by H. Bellen, Baylor College; Nolo et al., 2000), and rabbit anti-Mib1 (1:200; Le Borgne et al., 2005b). Anti-Ser, -Dl, and -N antibodies recognized extracellular epitopes. All secondary antibodies were Cy2-, Cy3-, and Cy5-coupled antibodies obtained from Jackson ImmunoResearch Laboratories, Inc.

Surface staining experiments were performed at 4°C. Third instar larvae wing discs were dissected at 4°C in Schneider (S2) medium and incubated for 2 h at 4°C with anti-Dl (C594.9B concentrate; 1:50; DSHB) and anti-Ser (1:50; provided by K. Irvine) in S2 medium. Discs were rinsed four times for 5 min at 4°C with S2 medium and fixed for 30 min at 4°C

in 4% PFA. Lectin HPA-TRITC (1:100; Sigma-Aldrich) surface staining was performed at 4°C with no detergent.

Anti-Dl uptake assays in pupal nota were performed as described previously (Le Borgne and Schweisguth, 2003). Pupal nota were dissected in Schneider's *Drosophila* medium (S2 medium; Invitrogen) and directly incubated for 8 min at 25°C with mouse monoclonal anti-Dl antibody C594-9B (concentrate from the DSHB; 1:50) that recognizes the extracellular portion of Dl. After rapid medium changes, nota were fixed and processed for immunostainings.

Anti-Dl uptake assays in wing imaginal discs were performed as described previously (Le Borgne et al., 2005b). Dissected discs were incubated with anti-Dl antibody C594-9B (concentrate from the DSHB; 1:50) at 4°C for 2 h. After rapid medium changes, discs were incubated in S2 medium without antibodies for 30 min at 25°C. Discs were fixed and processed for immunostainings. 50 µg/ml FM4-64FX (Invitrogen) uptake assays were performed as described for wing imaginal discs.

Secondary antibody staining followed standard protocols. Immunofluorescent preparations were mounted in 4% *N*-propyl-gallate and 80% glycerol and analyzed using confocal microscopes (SP2 and SPE; Leica) with 63× NA 1.3 and 100× NA 1.4 objectives (HCX Plan Apo CS; Leica). All high magnification views in Figs. 3–5, S2, and S3 are single confocal sections, whereas low magnification views in Figs. 1, 3–6, S2, and S3 are maximal projections of selected sections from confocal stacks. Wings and nota were mounted in Hoyer's medium and photographed using a macroscope (AZ100; Carl Zeiss, Inc.) or a microscope (DMRX2; Leica) equipped with a camera (FC420; Leica). ImageJ (National Institutes of Health) and Adobe softwares were used to prepare the figures.

GSL extraction

GSLs were extracted from frozen larvae as described previously (Wandall et al., 2005). 1 g frozen third instar larvae was thawed and homogenized (micropilon; Eppendorf) in 1.5 ml solvent A (2-isopropanol/hexane/water; 55:25:20 vol/vol/vol). The homogenate was centrifuged for 10 min at 2,000 rpm (GR-412; Jouan), and the supernatant was removed and kept. This step was repeated with 1.5 ml solvent B (chloroform/methanol; 1:1 vol/vol), 1.5 ml solvent A, and finally 1.5 ml solvent B. The four supernatant fractions (crude lipid extracts) were combined, evaporated under a nitrogen flux, and resuspended in chloroform/methanol (2:1 vol/vol) at a lipid concentration of 1 mg/ml. The extracts were evaporated, resuspended in 5 ml methanol containing 0.1 M NaOH, and incubated for 1 h at 37°C under agitation to remove most glycerolipid ester species (mild alkaline hydrolysis). The samples were dried by evaporation and re-extracted in chloroform/methanol (2:1 vol/vol). Neutral GSLs were finally purified on a column (DEAE-Sephadex A-25; Sigma-Aldrich), eluted with chloroform/methanol/water (30:60:8 vol/vol/vol), and analyzed by high performance thin layer chromatography (HPTLC) using silica gel 60 HPTLC plates (Merck) in chloroform/methanol/water (60:35:8 vol/vol/vol) as described previously (Fantini et al., 1993). The HPTLC plates were sprayed with orcinol and heated at 110°C for GSL detection. Standard GSLs were purchased from Matreya except for the Forssmann glycolipid (GalNAc-α1-3-GalNAc-β1-3Galα1-4Galbl-4Glcβ1-1Cer), which was purified from human erythrocytes.

Peptide–GSL interaction

Synthetic peptides (purity >95%) were purchased from Eurogentec. The Ser[1–288] and Ser[1–288]W180A proteins were produced in S2 cells transfected with the pMT-Ser[1–288] and pMT-Ser[1–288]W180A (these plasmids are derivatives by PCR cloning from the pMT-WB-Ser/AP plasmid described in Xu et al., 2007; cloning details are available upon request). S2 cells were grown in 500 ml serum-free Insect Express medium (Invitrogen) and were induced with 5 µm cadmium for 7 d. Secreted 6xHis-tagged proteins were purified using a metal affinity resin (TALON; Takara Bio Inc.), filtered using a column (Superdex 75; GE Healthcare), and concentrated in PBS to 1 mg/ml using a 3-kD column (Amikon).

Surface pressure measurements revealing peptide–GSL and protein–GSL interactions were studied as described previously (Fantini et al., 2006) by the Langmuir film balance technique with a fully automated microtensiometer (µTROUGH SX; Kibron Inc.). All experiments were performed in a controlled atmosphere at 20 ± 1°C. Monomolecular films of the indicated lipids were spread on pure water subphases (800 µl vol) from chloroform/methanol (1:1 vol/vol). After spreading of the film, 5 min was allowed for solvent evaporation. The initial surface pressure of these reconstituted monolayers was 12–15 mN/m. Increase in the surface pressure was followed kinetically by real-time surface pressure measurements after injecting the peptide (final concentration of 10 µM) or the Ser[1–288] protein (10 µg/ml) into the aqueous phase underneath the glycolipid monolayer until equilibrium was reached. The maximal surface pressure increase induced by the peptide (expressed in mN/m) is the difference measured between the initial and maximal surface pressure values. The data were analyzed with the FilmWareX program (version 3.57; Kibron Inc.). The accuracy of the system under our experimental conditions was ±0.25 mN/m for surface pressure.

Online supplemental material

Figs. S1–S3 provide additional data on the phenotypes induced by dominant-negative Mib1^{C1205S}. Immunostainings in Fig. S1 reveal that Mib1^{C1205S} does not perturb the distribution of junctional proteins. Clone analysis in Fig. S2 show that the Mib1-dependent defects in Notch localization require Dl and/or Ser. Cell surface stainings in Fig. S3 show that Dl and Ser localize at the surface of Mib1^{C1205S}-expressing cells. Online supplemental material is available at http://www.jcb.org/cgi/content/full/jcb.200907116/DC1.

We thank H. Bellen, P. Bryant, K. Choi, N. Haines, K. Irvine, U. Tepass, R. Ueda, the Bloomington and Szeged Stock Centers, the Vienna *Drosophila* RNAi Center, the *Drosophila* Genomics Ressource Center, the *Drosophila* Tilling Project, and DSHB for flies, antibodies, and plasmids. We are particularly thankful to M. Tomaru and M. Yamamoto of the *Drosophila* Genetic Ressource Center for the Gene Search lines. We thank O. Beaudouin, C.G. Blavet, L. Couturier, E. Crublet, S. Heuss, M. Keita, E. Kubiaczyk, R. Le Borgne, F. Logeat, and V. Mayau for help and advice. We also thank all laboratory members for discussion and comments on the manuscript.

This work was funded by core funding from the Institut Pasteur and Centre National de la Recherche Scientifique and by specific grants from L'Agence Nationale de la Recherche (grant 05-BLAN-0277) and L'Association pour la Recherche sur le Cancer (ARC; grant 3415). S.Hamel received doctoral fellowships from the French ministry of education, research, and technology and the ARC.

Submitted: 20 July 2009
Accepted: 25 January 2010

References

Bardin, A.J., and F. Schweisguth. 2006. Bearded family members inhibit Neuralized-mediated endocytosis and signaling activity of Delta in *Drosophila*. *Dev. Cell.* 10:245–255. doi:10.1016/j.devcel.2005.12.017

Bhat, M.A., S. Izaddoost, Y. Lu, K.O. Cho, K.W. Choi, and H.J. Bellen. 1999. Discs Lost, a novel multi-PDZ domain protein, establishes and maintains epithelial polarity. *Cell.* 96:833–845. doi:10.1016/S0092-8674(00)80593-0

Bray, S.J. 2006. Notch signalling: a simple pathway becomes complex. *Nat. Rev. Mol. Cell Biol.* 7:678–689. doi:10.1038/nrm2009

Chen, W., and D. Casey Corliss. 2004. Three modules of zebrafish Mind bomb work cooperatively to promote Delta ubiquitination and endocytosis. *Dev. Biol.* 267:361–373. doi:10.1016/j.ydbio.2003.11.010

Chen, Y.W., J.W. Pedersen, H.H. Wandall, S.B. Levery, S. Pizette, H. Clausen, and S.M. Cohen. 2007. Glycosphingolipids with extended sugar chain have specialized functions in development and behavior of *Drosophila*. *Dev. Biol.* 306:736–749. doi:10.1016/j.ydbio.2007.04.013

Cooper, J.L., E.A. Greene, B.J. Till, C.A. Codomo, B.T. Wakimoto, and S. Henikoff. 2008. Retention of induced mutations in a *Drosophila* reverse-genetic resource. *Genetics.* 180:661–667. doi:10.1534/genetics.108.092437

Crosnier, C., C. Driancourt, N. Raynaud, S. Dhorne-Pollet, N. Pollet, O. Bernard, M. Hadchouel, and M. Meunier-Rotival. 1999. Mutations in JAGGED1 gene are predominantly sporadic in Alagille syndrome. *Gastroenterology.* 116:1141–1148. doi:10.1016/S0016-5085(99)70017-X

D'Souza, B., A. Miyamoto, and G. Weinmaster. 2008. The many facets of Notch ligands. *Oncogene.* 27:5148–5167. doi:10.1038/onc.2008.229

Degroote, S., J. Wolthoorn, and G. van Meer. 2004. The cell biology of glycosphingolipids. *Semin. Cell Dev. Biol.* 15:375–387. doi:10.1016/j.semcdb.2004.03.007

Fantini, J., D.G. Cook, N. Nathanson, S.L. Spitalnik, and F. Gonzalez-Scarano. 1993. Infection of colonic epithelial cell lines by type 1 human immunodeficiency virus is associated with cell surface expression of galactosylceramide, a potential alternative gp120 receptor. *Proc. Natl. Acad. Sci. USA.* 90:2700–2704. doi:10.1073/pnas.90.7.2700

Fantini, J., N. Garmy, and N. Yahi. 2006. Prediction of glycolipid-binding domains from the amino acid sequence of lipid raft-associated proteins: application to HpaA, a protein involved in the adhesion of *Helicobacter pylori* to gastrointestinal cells. *Biochemistry.* 45:10957–10962. doi:10.1021/bi060762s

Fehon, R.G., K. Johansen, I. Rebay, and S. Artavanis-Tsakonas. 1991. Complex cellular and subcellular regulation of notch expression during embryonic

and imaginal development of *Drosophila*: implications for notch function. *J. Cell Biol.* 113:657–669. doi:10.1083/jcb.113.3.657

Fortini, M.E. 2009. Notch signaling: the core pathway and its posttranslational regulation. *Dev. Cell.* 16:633–647. doi:10.1016/j.devcel.2009.03.010

Golic, K.G., and M.M. Golic. 1996. Engineering the *Drosophila* genome: chromosome rearrangements by design. *Genetics.* 144:1693–1711.

Goode, S., M. Melnick, T.B. Chou, and N. Perrimon. 1996. The neurogenic genes egghead and brainiac define a novel signaling pathway essential for epithelial morphogenesis during *Drosophila* oogenesis. *Development.* 122:3863–3879.

Griffitts, J.S., S.M. Haslam, T. Yang, S.F. Garczynski, B. Mulloy, H. Morris, P.S. Cremer, A. Dell, M.J. Adang, and R.V. Aroian. 2005. Glycolipids as receptors for *Bacillus thuringiensis* crystal toxin. *Science.* 307:922–925. doi:10.1126/science.1104444

Haines, N., and K.D. Irvine. 2005. Functional analysis of *Drosophila* beta1,4-N-acetylgalactosaminyltransferases. *Glycobiology.* 15:335–346. doi:10.1093/glycob/cwi017

Hancock, J.F. 2006. Lipid rafts: contentious only from simplistic standpoints. *Nat. Rev. Mol. Cell Biol.* 7:456–462. doi:10.1038/nrm1925

Hebbar, S., E. Lee, M. Manna, S. Steinert, G.S. Kumar, M. Wenk, T. Wohland, and R. Kraut. 2008. A fluorescent sphingolipid binding domain peptide probe interacts with sphingolipids and cholesterol-dependent raft domains. *J. Lipid Res.* 49:1077–1089. doi:10.1194/jlr.M700543-JLR200

Heuss, S.F., D. Ndiaye-Lobry, E.M. Six, A. Israël, and F. Logeat. 2008. The intracellular region of Notch ligands Dll1 and Dll3 regulates their trafficking and signaling activity. *Proc. Natl. Acad. Sci. USA.* 105:11212–11217. doi:10.1073/pnas.0800695105

Iskratsch, T., A. Braun, K. Paschinger, and I.B. Wilson. 2009. Specificity analysis of lectins and antibodies using remodeled glycoproteins. *Anal. Biochem.* 386:133–146. doi:10.1016/j.ab.2008.12.005

Itoh, M., C.H. Kim, G. Palardy, T. Oda, Y.J. Jiang, D. Maust, S.Y. Yeo, K. Lorick, G.J. Wright, L. Ariza-McNaughton, et al. 2003. Mind bomb is a ubiquitin ligase that is essential for efficient activation of Notch signaling by Delta. *Dev. Cell.* 4:67–82. doi:10.1016/S1534-5807(02)00409-4

Katic, I., L.G. Vallier, and I. Greenwald. 2005. New positive regulators of lin-12 activity in *Caenorhabditis elegans* include the BRE-5/Brainiac glycosphingolipid biosynthesis enzyme. *Genetics.* 171:1605–1615. doi:10.1534/genetics.105.048041

Kooh, P.J., R.G. Fehon, and M.A. Muskavitch. 1993. Implications of dynamic patterns of Delta and Notch expression for cellular interactions during *Drosophila* development. *Development.* 117:493–507.

Kopan, R., and M.X. Ilagan. 2009. The canonical Notch signaling pathway: unfolding the activation mechanism. *Cell.* 137:216–233. doi:10.1016/j.cell.2009.03.045

Lai, E.C., F. Roegiers, X. Qin, Y.N. Jan, and G.M. Rubin. 2005. The ubiquitin ligase *Drosophila* Mind bomb promotes Notch signaling by regulating the localization and activity of Serrate and Delta. *Development.* 132:2319–2332. doi:10.1242/dev.01825

Lajoie, P., J.G. Goetz, J.W. Dennis, and I.R. Nabi. 2009. Lattices, rafts, and scaffolds: domain regulation of receptor signaling at the plasma membrane. *J. Cell Biol.* 185:381–385. doi:10.1083/jcb.200811059

Le Borgne, R., and F. Schweisguth. 2003. Unequal segregation of Neuralized biases Notch activation during asymmetric cell division. *Dev. Cell.* 5:139–148. doi:10.1016/S1534-5807(03)00187-4

Le Borgne, R., A. Bardin, and F. Schweisguth. 2005a. The roles of receptor and ligand endocytosis in regulating Notch signaling. *Development.* 132:1751–1762. doi:10.1242/dev.01789

Le Borgne, R., S. Remaud, S. Hamel, and F. Schweisguth. 2005b. Two distinct E3 ubiquitin ligases have complementary functions in the regulation of delta and serrate signaling in *Drosophila*. *PLoS Biol.* 3:e96. doi:10.1371/journal.pbio.0030096

Lingwood, D., and K. Simons. 2010. Lipid rafts as a membrane-organizing principle. *Science.* 327:46–50. doi:10.1126/science.1174621

Lingwood, D., J. Ries, P. Schwille, and K. Simons. 2008. Plasma membranes are poised for activation of raft phase coalescence at physiological temperature. *Proc. Natl. Acad. Sci. USA.* 105:10005–10010. doi:10.1073/pnas.0804374105

Mahfoud, R., N. Garmy, M. Maresca, N. Yahi, A. Puigserver, and J. Fantini. 2002. Identification of a common sphingolipid-binding domain in Alzheimer, prion, and HIV-1 proteins. *J. Biol. Chem.* 277:11292–11296. doi:10.1074/jbc.M111679200

Maresca, M., A. Derghal, C. Carravagna, S. Dudin, and J. Fantini. 2008. Controlled aggregation of adenine by sugars: physicochemical studies, molecular modelling simulations of sugar-aromatic CH-pi stacking interactions, and biological significance. *Phys. Chem. Chem. Phys.* 10:2792–2800. doi:10.1039/b802594k

Müller, R., F. Altmann, D. Zhou, and T. Hennet. 2002. The *Drosophila melanogaster* brainiac protein is a glycolipid-specific beta 1,3N-acetylglucosaminyltransferase. *J. Biol. Chem.* 277:32417–32420. doi:10.1074/jbc.C200381200

Nolo, R., L.A. Abbott, and H.J. Bellen. 2000. Senseless, a Zn finger transcription factor, is necessary and sufficient for sensory organ development in *Drosophila. Cell.* 102:349–362. doi:10.1016/S0092-8674(00)00040-4

North, S.J., K. Koles, C. Hembd, H.R. Morris, A. Dell, V.M. Panin, and S.M. Haslam. 2006. Glycomic studies of *Drosophila melanogaster* embryos. *Glycoconj. J.* 23:345–354. doi:10.1007/s10719-006-6693-4

Oda, H., T. Uemura, Y. Harada, Y. Iwai, and M. Takeichi. 1994. A *Drosophila* homolog of cadherin associated with armadillo and essential for embryonic cell-cell adhesion. *Dev. Biol.* 165:716–726. doi:10.1006/dbio.1994.1287

Papayannopoulos, V., A. Tomlinson, V.M. Panin, C. Rauskolb, and K.D. Irvine. 1998. Dorsal-ventral signaling in the *Drosophila* eye. *Science.* 281:2031–2034. doi:10.1126/science.281.5385.2031

Parks, A.L., J.R. Stout, S.B. Shepard, K.M. Klueg, A.A. Dos Santos, T.R. Parody, M. Vaskova, and M.A. Muskavitch. 2006. Structure-function analysis of delta trafficking, receptor binding and signaling in *Drosophila. Genetics.* 174:1947–1961. doi:10.1534/genetics.106.061630

Pizette, S., C. Rabouille, S.M. Cohen, and P. Thérond. 2009. Glycosphingolipids control the extracellular gradient of the *Drosophila* EGFR ligand Gurken. *Development.* 136:551–561. doi:10.1242/dev.031104

Protzer, C.E., A. Preiss, and A.C. Nagel. 2009. *Drosophila* alpha-1,4-glycosyltransferase (alpha-4GT1) inhibits reaper-mediated apoptosis in the eye. *Cell Tissue Res.* 336:149–158. doi:10.1007/s00441-009-0758-1

Röpke, A., A. Kujat, M. Gräber, J. Giannakudis, and I. Hansmann. 2003. Identification of 36 novel Jagged1 (JAG1) mutations in patients with Alagille syndrome. *Hum. Mutat.* 21:100. doi:10.1002/humu.9102

Sanchez, J.F., J. Lescar, V. Chazalet, A. Audfray, J. Gagnon, R. Alvarez, C. Breton, A. Imberty, and E.P. Mitchell. 2006. Biochemical and structural analysis of Helix pomatia agglutinin. A hexameric lectin with a novel fold. *J. Biol. Chem.* 281:20171–20180. doi:10.1074/jbc.M603452200

Sasaki, N., T. Sasamura, H.O. Ishikawa, M. Kanai, R. Ueda, K. Saigo, and K. Matsuno. 2007. Polarized exocytosis and transcytosis of Notch during its apical localization in *Drosophila* epithelial cells. *Genes Cells.* 12:89–103. doi:10.1111/j.1365-2443.2007.01037.x

Seppo, A., M. Moreland, H. Schweingruber, and M. Tiemeyer. 2000. Zwitterionic and acidic glycosphingolipids of the *Drosophila melanogaster* embryo. *Eur. J. Biochem.* 267:3549–3558. doi:10.1046/j.1432-1327.2000.01383.x

Sharma, D.K., J.C. Brown, A. Choudhury, T.E. Peterson, E. Holicky, D.L. Marks, R. Simari, R.G. Parton, and R.E. Pagano. 2004. Selective stimulation of caveolar endocytosis by glycosphingolipids and cholesterol. *Mol. Biol. Cell.* 15:3114–3122. doi:10.1091/mbc.E04-03-0189

Sillence, D.J. 2007. New insights into glycosphingolipid functions—storage, lipid rafts, and translocators. *Int. Rev. Cytol.* 262:151–189. doi:10.1016/S0074-7696(07)62003-8

Singh, R.D., E.L. Holicky, Z.J. Cheng, S.Y. Kim, C.L. Wheatley, D.L. Marks, R. Bittman, and R.E. Pagano. 2007. Inhibition of caveolar uptake, SV40 infection, and β1-integrin signaling by a nonnatural glycosphingolipid stereoisomer. *J. Cell Biol.* 176:895–901. doi:10.1083/jcb.200609149

Stolz, A., N. Haines, A. Pich, K.D. Irvine, C.H. Hokke, A.M. Deelder, R. Gerardy-Schahn, M. Wuhrer, and H. Bakker. 2008. Distinct contributions of beta 4GalNAcTA and beta 4GalNAcTB to *Drosophila* glycosphingolipid biosynthesis. *Glycoconj. J.* 25:167–175. doi:10.1007/s10719-007-9069-5

Tepass, U., and E. Knust. 1993. Crumbs and stardust act in a genetic pathway that controls the organization of epithelia in *Drosophila melanogaster. Dev. Biol.* 159:311–326. doi:10.1006/dbio.1993.1243

Tien, A.C., A. Rajan, and H.J. Bellen. 2009. A Notch updated. *J. Cell Biol.* 184:621–629. doi:10.1083/jcb.200811141

Toba, G., T. Ohsako, N. Miyata, T. Ohtsuka, K.H. Seong, and T. Aigaki. 1999. The gene search system. A method for efficient detection and rapid molecular identification of genes in *Drosophila melanogaster. Genetics.* 151:725–737.

Wandall, H.H., J.W. Pedersen, C. Park, S.B. Levery, S. Pizette, S.M. Cohen, T. Schwientek, and H. Clausen. 2003. *Drosophila* egghead encodes a beta 1,4-mannosyltransferase predicted to form the immediate precursor glycosphingolipid substrate for brainiac. *J. Biol. Chem.* 278:1411–1414. doi:10.1074/jbc.C200619200

Wandall, H.H., S. Pizette, J.W. Pedersen, H. Eichert, S.B. Levery, U. Mandel, S.M. Cohen, and H. Clausen. 2005. Egghead and brainiac are essential for glycosphingolipid biosynthesis in vivo. *J. Biol. Chem.* 280:4858–4863. doi:10.1074/jbc.C400571200

Weber, U., C. Eroglu, and M. Mlodzik. 2003. Phospholipid membrane composition affects EGF receptor and Notch signaling through effects on

endocytosis during *Drosophila* development. *Dev. Cell.* 5:559–570. doi:10.1016/S1534-5807(03)00273-9

Xu, A., N. Haines, M. Dlugosz, N.A. Rana, H. Takeuchi, R.S. Haltiwanger, and K.D. Irvine. 2007. In vitro reconstitution of the modulation of *Drosophila* Notch-ligand binding by Fringe. *J. Biol. Chem.* 282:35153–35162. doi:10.1074/jbc.M707040200

Yoon, S.J., K. Nakayama, T. Hikita, K. Handa, and S.I. Hakomori. 2006. Epidermal growth factor receptor tyrosine kinase is modulated by GM3 interaction with N-linked GlcNAc termini of the receptor. *Proc. Natl. Acad. Sci. USA.* 103:18987–18991. doi:10.1073/pnas.0609281103

Zhang, C., Q. Li, C.H. Lim, X. Qiu, and Y.J. Jiang. 2007. The characterization of zebrafish antimorphic mib alleles reveals that Mib and Mind bomb-2 (Mib2) function redundantly. *Dev. Biol.* 305:14–27. doi:10.1016/j.ydbio.2007.01.034